

Man-in-the-Middle Attack against Object Detection Systems

Han Wu, Sareh Rowlands and Johan Wahlstrom*

Abstract—Is deep learning secure for robots? As embedded systems have access to more powerful CPUs and GPUs, deep-learning-enabled object detection systems become pervasive in robotic applications. Meanwhile, prior research unveils that deep learning models are vulnerable to adversarial attacks. Does this put real-world robots at threat? Our research borrows the idea of the Main-in-the-Middle attack from Cryptography to attack an object detection system. Our experimental results prove that we can generate a strong Universal Adversarial Perturbation (UAP) within one minute and then use the perturbation to attack a detection system via the Man-in-the-Middle attack. Our findings raise a serious concern over the applications of deep learning models in safety-critical systems such as autonomous driving.

I. INTRODUCTION

Advances in deep neural networks have opened a new era of robotics, intelligent robots. Intelligent robots possess a more comprehensive perception of environments. However, it's no more a secret that deep neural networks are vulnerable to adversarial attacks. Does this mean deep-learning-enabled object detection systems are no more secure for safety-critical applications?

It has been eight years since the first adversarial attack against neural networks. Goodfellow et al. [1] (2014) fooled an image classification model by adding a small perturbation to the input image. The perturbation is unperceivable by human eyes but can lead the deep learning model to wrong classification results. Lu et al. [2] (2017) extend the attack from classification models to detection models and apply the attack to an autonomous driving car. Their experiments showed that the autonomous vehicle only misclassified traffic signs placed within a small distance and viewed from specific angles. Thus, it is more challenging to attack real-world robots working in a dynamic environment.

It is still unclear how adversarial attacks could affect real-world robotic applications such as autonomous vehicles. In the past five years, more research has focused on attacking object detection models deployed in autonomous driving systems. So far, adversarial attacks fall into two categories: digital attacks and physical attacks. Digital attacks apply the perturbation directly to the digital input image. On the other hand, physical attacks print the perturbation on physical objects such as a poster [3] or a T-shirt [4].

However, both digital attacks and physical attacks have their limitations. Digital perturbation requires access to the detection system to add the perturbation internally. Under

Han Wu, Sareh Rowlands and Johan Wahlstrom are with the University of Exeter, Stocker Rd, Exeter EX4 4PY, the UK (hw630@exeter.ac.uk; s.rowlands@exeter.ac.uk; j.wahlstrom@exeter.ac.uk).

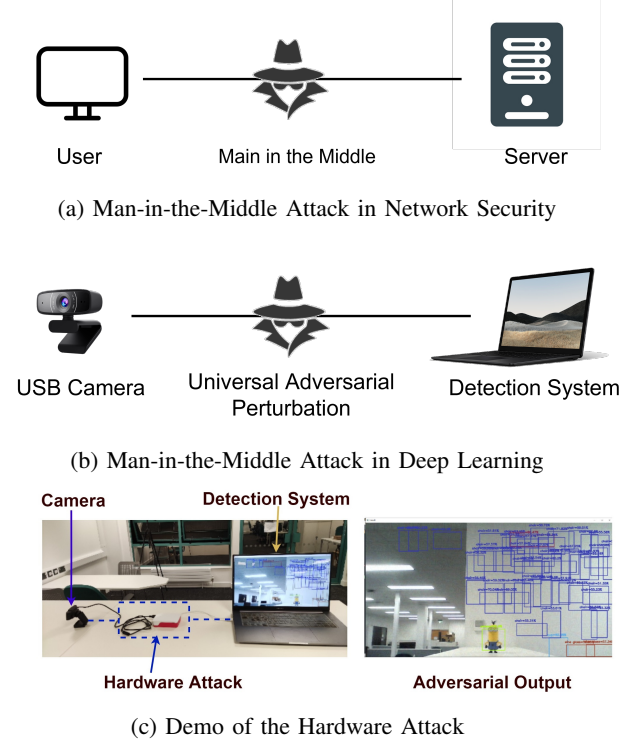


Fig. 1: Overview of Man-in-the-Middle Attack

real-world scenarios, it is not trivial to hack into the Google Self-Driving Car and apply the attack. Physical attack is susceptible to position and angle variations, and it is inflexible. Once we print out the adversarial poster, we cannot change it unless reprinting. During the trial-and-error process, massive reprinting wastes time and resources.

In this research, we introduce a new hardware attack, Man-in-the-Middle Attack, that combines digital and physical attacks. The idea is inspired by Man-in-the-Middle Attack in network security, where the attacker eavesdrops and manipulates the data transferred between the user and the server (see Figure 1). Overall, this paper makes the following contributions and our source code is available here ¹:

- 1) **The Hardware Attack:** We introduce a new category of attack that is flexible and easy to deploy.
- 2) **The White-box Adversarial Toolbox:** We design an open-source python toolbox for adversarial attacks.
- 3) **New Evaluation Metrics:** We propose three evaluation metrics that help to achieve strong attacks.

¹The source code is available on Github: <https://github.com/wuhanstudio/adversarial-camera>

II. PRELIMINARIES

This section introduces the most widely-deployed object detection models and existing adversarial attacks against these models.

A. Object Detection Models

The object detection task needs to locate the position and classify the category of each object in an image. Thus we need to solve two problems: localization and classification. Depending on how we solve these two problems, simultaneously or separately, we can divide existing object detection models into two categories: one-stage and two-stage methods. Zhao et al. also describe one-stage methods as regression / classification-based methods and two-stage methods as region proposal-based methods [5].

One-stage methods regard object detection as a classification or regression task that outputs locations and categories simultaneously in a single run, making it computationally efficient. YOLO [6] and SSD [7] are the two most widely deployed one-stage models in embedded systems. They can achieve real-time performance on CPUs without GPUs, which is an advantage for embedded systems.

Two-stage methods consist of two steps: first, they generate a series of region proposals and then classify each proposal into different categories. Faster RCNN [8] and Mask RCNN [9] are the two most well-known two-stage methods. Besides, Mask RCNN can also solve the image segmentation task that assigns labels for each pixel instead of just output bounding boxes.

For robotic applications, one-stage methods are more popular because they are faster, and the accuracy is acceptable in most cases. Two-stage methods are generally more accurate but computationally expensive. More powerful GPUs require better cooling systems which may not be available on embedded systems. Besides, intensive computation requires more electricity and a larger battery, which could also become the bottleneck for real-time robotic applications.

However, both one-stage and two-stage models are vulnerable to adversarial attacks. In this research, we intend to investigate how these attacks affect real-time robotic applications. As a result, we focus on the more efficient one-stage models, YOLO and SSD.

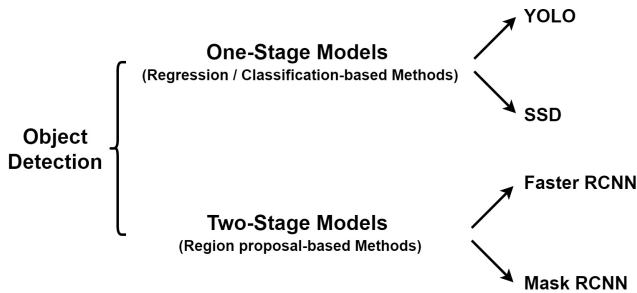


Fig. 2: Most widely used Object Detection Models

B. Universal Adversarial Perturbation (UAPs)

In 2014, Goodfellow et al. published the first adversarial attack against classification models using the Fast Gradient Sign Method (FGSM) [1]. This method uses gradients to generate image-specific perturbations. If the input image changes, the perturbation needs to be regenerated. For real-world robotic applications in dynamic environments, it is more practical to use image-agnostic perturbations.

In 2017, Moosavi-Dezfooli et al. fool classification models on most images in a dataset using a single perturbation. Such image-agnostic perturbations are also known as Universal Adversarial Perturbations (UAPs). Later, researchers extend adversarial attacks from image classification to image segmentation [10] and detection models [11].

Besides image-specific and image-agnostic methods, we can also classify adversarial attacks into data-driven and data-independent approaches. Data-driven approaches require access to the input image, while data-independent methods only need access to the parameters and architecture of the target model. Data-driven approaches achieve a higher fooling rate as they have more information.

Data-driven methods include Gradient-based Methods, Generative Adversarial Networks (GANs), and Optimization-based Methods. Gradient-based methods use gradients to maximize adversarial loss rather than minimize the training loss. Different methods design different adversarial loss functions [12][13][14]. Some researchers also train GANs to generate adversarial examples [15][16]. We can also transform the attack problem into an optimization problem that minimizes the perturbation while maximizing the training loss and then use existing optimizers to solve [17][18].

Additionally, we can use data-driven methods to generate physical perturbations by adding extra constraints [3]. For example, we can add the Sub-sampled Non-Printability Score (SNPS) constraint to the loss function. The Non-Printability Score (NPS) measures the error between a printed pixel and its digital counterparts. With additional constraints, we can generate physical perturbations that preserve the adversarial effect if printed out on a poster.

In the next section, we devise our gradient-based data-driven method that generates image-agnostic UAPs and then applies the perturbation via the Man-in-the-Middle attack.

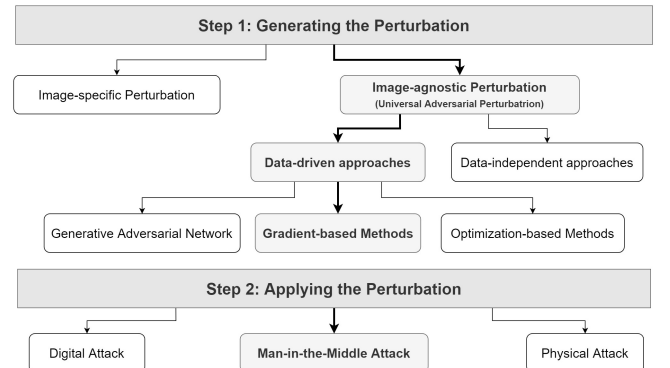


Fig. 3: Generating and Applying Adversarial Perturbations

III. MAN-IN-THE-MIDDLE ATTACK

This section introduces how we devise a gradient-based method, named as the PCB attack, to generate the Universal Adversarial Perturbation (UAP). We then apply the perturbation via a novel hardware attack inspired by the Man-in-the-Middle Attack in cryptography.

A. Problem Formulation

First, we give the mathematical formulation of adversarial attacks against object detection. As introduced in Section II, existing object detection models consist of one-stage models (YOLO, SSD) and two-stage models (Faster-RCNN, Mask-RCNN). Though different models have different structures, they share similar inputs and outputs.

We use the following notations throughout the paper:

- x : The original clean input image.
- δ : The adversarial perturbation.
- x' : The adversarial input image $x' = x + \delta$.
- K : Total number of candidate classes.
- N : Total number of candidate bounding boxes.
- $\mathcal{O}(x)$: The ground truth of the input image x .
- $\hat{\mathcal{O}}(x)$: The output of N candidate bounding boxes from the model given the input image x . $\hat{\mathcal{O}}(x) = \{\hat{o}_1, \hat{o}_2, \hat{o}_3, \dots, \hat{o}_N\}$.
- $\hat{o}_i(x)$: The i_{th} output in $\hat{\mathcal{O}}(x)$, and $\hat{o}_i = (\hat{b}_i, \hat{c}_i, \hat{p}_i)$. $1 \leq i \leq N$.
- \hat{b}_i : The location and dimension of the i_{th} candidate box. $\hat{b}_i = (\hat{b}_i^x, \hat{b}_i^y, \hat{b}_i^w, \hat{b}_i^h)$ that represents a bounding box at position $(\hat{b}_i^x, \hat{b}_i^y)$ with width \hat{b}_i^w and height \hat{b}_i^h .
- \hat{c}_i : The confidence value (objectness) of the i_{th} candidate box that represents how likely there is an object.
- \hat{p}_i : The softmax probability vector of the i_{th} candidate box. $\hat{p}_i = (\hat{p}_i^1, \hat{p}_i^2, \dots, \hat{p}_i^K)$ for K classes and $\sum \hat{p}_i = 1$.

Putting things together: Given an input image x , the object detection model outputs N candidate bounding boxes. $\hat{\mathcal{O}}(x) = \{\hat{o}_1, \hat{o}_2, \hat{o}_3, \dots, \hat{o}_N\}$. Each candidate box $\hat{o}_i = (\hat{b}_i, \hat{c}_i, \hat{p}_i)$ contains $\hat{b}_i = (\hat{b}_i^x, \hat{b}_i^y, \hat{b}_i^w, \hat{b}_i^h)$ that represents the location and dimension of the box, the confidence value $\hat{c}_i \in [0, 1]$ that represents how likely there is an object, and the softmax probability vector, $\hat{p}_i = (\hat{p}_i^1, \hat{p}_i^2, \dots, \hat{p}_i^K)$ for K classes. The raw outputs from the detection model $\hat{\mathcal{O}}(x)$ may contain several thousand candidate bounding boxes. We then use the Non-maximum Suppression (NMS) method [19] to filter out bounding boxes with low confidence values or high Intersection over Union (IoU) to generate final detection results.

An adversarial example x' aims to fool the detection model so that it outputs different candidate boxes $\hat{\mathcal{O}}(x') \neq \hat{\mathcal{O}}(x)$. For example, the adversarial output $\hat{\mathcal{O}}(x')$ may detect more false positive objects after the NMS. Meanwhile, the perturbation δ , defined as the difference between the original clean input x and the adversarial input x' is bounded by the L_p norm such that the perturbation is unperceivable by human eyes. This can be formulated as:

$$\min \|x' - x\|_p \quad s.t. \quad \hat{\mathcal{O}}(x') \neq \hat{\mathcal{O}}(x) \quad (1)$$

B. Generating the perturbation (PCB Attack)

Gradient-based methods use similar approaches to generate image-specific and image-agnostic perturbations. Given one input image, we iterate over a single image to produce an image-specific perturbation; Given the entire dataset, we then iterate over multiple images to generate the UAP. Thus, we first introduce how we generate image-specific perturbations and then extend the attack to its image-agnostic counterpart.

We name our attack the PCB attack because we handle the output of probability vector (P), confidence value (C), and bounding boxes separately (B). Besides, the acronym of PCB gives us a feeling of a hardware attack that shares the same acronym with Printed Circuit Board (PCB).

1) **Image-specific PCB Attack**: The intuition behind gradient-based methods is straightforward. Our objective is to fool the detection model to make inaccurate predictions. We minimize the training loss to train an accurate model. If we maximize the training loss, we produce adversarial predictions. The training loss is a function of the input x , the model weights \mathcal{W} , and the ground truth \mathcal{O} . During the training process, we minimize the training loss by updating model weights.

$$\min \mathcal{L}_{train} = f(\mathcal{W}; x, \mathcal{O}) \quad (2)$$

$$\max \mathcal{L}_{adv} = f(x, \mathcal{O}^*; \mathcal{W}) \quad (3)$$

For the attacker, we cannot change the model weights, thus we maximize the training loss by updating the input x and replacing the ground truth with desired adversarial outputs \mathcal{O}^* . We first zero-initialize the perturbation δ , then use Projected Gradient Descent (PGD) [20] with learning rate decay to update the perturbation. Different gradient-based methods use different adversarial loss functions \mathcal{L}_{adv} and construct desired adversarial outputs \mathcal{O}^* differently.

$$\delta_{t+1} = \text{proj}_p(\delta_t + \alpha \text{sign}(\frac{\partial \mathcal{L}_{adv}(x'_t; \mathcal{O}^*)}{\partial x'_t})) \quad (4)$$

In our attack, we separate the Probability vector and Confidence value (PC) with Bounding boxes (B) and produce two adversarial loss functions. If we maximize the adversarial loss, we generate large amounts of incorrect bounding boxes (Fabrication attack); If we minimize the loss, we diminish all the bounding boxes (Vanishing attack). We summarize the image-specific PCB attack in the algorithm 1.

$$\mathcal{L}_{PC}(x) = \sum \sigma(c_i) * \sigma(p_i) \quad (5)$$

$$\mathcal{L}_{PCB}(x) = \frac{\sum (\sigma(c_i) * \sigma(p_i))}{\sum [\sigma(w_i) * \sigma(h_i)]^2} \quad (6)$$

2) **Image-agnostic PCB Attack**: We can extend the method to an image-agnostic attack by iterating over a collection of images. X_s represents all available sample images to the attacker. X_s can be the training set or a video clip from the target scene.

In each iteration, we iterate the perturbation δ over X_s . The learning rate α should be relatively small compared to the image-specific PCB attack. We summarize the image-agnostic PCB attack in the algorithm 2 and discuss how we choose hyper-parameters in the next section.

Algorithm 1 Image-specific PCB Attack

Input: The target model, the input image $x \in [0, 1]$.
Parameters: Learning rate α , learning rate decay k , number of iterations n , the strength of the attack ϵ bounded by l_p norm.
Output: Image-specific perturbation δ
Initialize $\delta \leftarrow 0$
for $i = 1 : n$ **do**
 $x' = x + \delta$
 $\nabla = \frac{\partial L_{adv}^*(x')}{\partial x'}$
 $\delta \leftarrow \delta + \alpha * \text{sign}(\nabla)$
 $\delta \leftarrow \text{clip}(-1, 1)$
 $\delta \leftarrow \text{proj-p}(\delta, \epsilon)$
 $\alpha = \alpha * k$ \triangleright The learning rate decay is important
end for

Algorithm 2 Image-agnostic PCB Attack (UAP)

Input: The target model, the input image $x \in [0, 1]$, the sample images X_s .
Parameters: Learning rate α , learning rate decay k , number of iterations n , the strength of the attack ϵ bounded by l_p norm.
Output: Image-specific perturbation δ
Initialize $\delta \leftarrow 0$
for $i = 1 : n$ **do**
 for each image $x \in X_s$ **do**
 $x' = x + \delta$
 $\nabla = \frac{\partial L_{adv}^*(x')}{\partial x'}$
 $\delta \leftarrow \delta + \alpha * \text{sign}(\nabla)$ $\triangleright \alpha$ is very small
 $\delta \leftarrow \text{clip}(-1, 1)$
 $\delta \leftarrow \text{proj-p}(\delta, \epsilon)$
 end for
 $\alpha = \alpha * k$
end for

C. Applying the perturbation (Man-in-the-Middle Attack)

In Section I, we mention that the biggest hurdle for the digital attack is not having access to the internal system. The perturbation is the same size as the model input (YOLO 416x416) because we generate it using the gradient of the model input over the adversarial loss. However, in real-world applications, the resized image is a temporary variable in the middle of the detection system. Thus, we need to hack into the operating system and inject malicious code into the embedded system, which is not trivial.

To solve this problem, we devise the Man-in-the-Middle Hardware Attack. We notice that the sensor (camera) that captures the image is exposed directly to the outside world

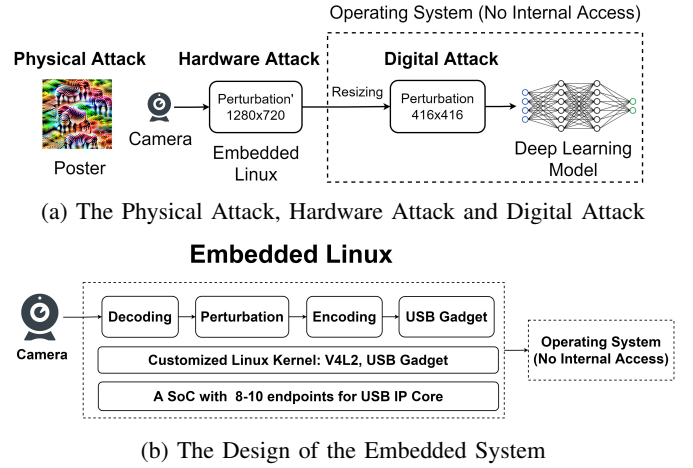


Fig. 4: The System Architecture

without any protection. If we eavesdrop and manipulate the image data between the sensor and the detection system, we can apply the perturbation without access to the internal system.

1) **Hardware Implementation:** On the one side, we need hardware that reads raw images from the USB camera and injects the perturbation. On the other side, it simulates a virtual camera to the detection system. In this way, the operating system has no idea that the camera is under attack because it still detects a USB camera device.

There is a lot of hardware capable of reading images from a USB camera, but it is more challenging to simulate a virtual USB camera. We find Raspberry Pi Zero, Raspberry Pi 4, and IMX6UL satisfies the requirement. Besides, a proper Linux Kernel that supports V4L2 Driver, USB Gadget Framework, and Configfs is required to drive the hardware. We illustrate the overall architecture of the system design in figure 4.

2) **Resizing the perturbation:** If we move the perturbation from the input of the model to the outside of the detection system, the perturbation is applied before preprocessing (resizing). For example, the input shape of YOLO and the perturbation is 416x416. However, the image shape of a USB camera could be 1280x720.

Formally, if we use \mathcal{R} to denote the resize function that downscales an image ($1280 \times 720 \rightarrow 416 \times 416$), and \mathcal{R}^{-1} to denote the one that upscales an image ($416 \times 416 \rightarrow 1280 \times 720$). The following equation holds for image resizing functions that use bilinear interpolation:

$$\mathcal{R}(x') = \mathcal{R}(x + \mathcal{R}^{-1}(\delta)) = \mathcal{R}(x) + \mathcal{R}\mathcal{R}^{-1}(\delta) \quad (7)$$

However, after resizing, the adversarial input constructed by Man-in-the-Middle attack is different from a valid adversarial input $\mathcal{R}(x) + \delta$:

$$\mathcal{R}(x) + \mathcal{R}\mathcal{R}^{-1}(\delta) \neq \mathcal{R}(x) + \delta \quad (8)$$

Our experimental results demonstrate that the effect of adversarial reserves even though the resize function is not invertible.



(a) Cannot distinguish different attacks: The fabrication attack (left) generates more objects, and the vanishing attack (right) clears detection results. None of them matches the ground truth. Thus, different attacks result in the same low mAP.



(b) Cannot highlight a stronger attack: Both strong (left) and weak (right) attacks produce an incorrect bounding box. The attacker prefers a strong attack (Dog 99%) over a weak attack (Dog 60%), but the mAP does not reflect the attack strength.

Fig. 5: Why the mAP is not suitable to evaluate attacks

IV. EXPERIMENTAL EVALUATION

A. Evaluation Metrics

Object Detection models use the Mean Accuracy Precision (mAP) [21] to measure the accuracy of detection results. Prior research also uses the mAP to evaluate the strength of adversarial attacks. However, we notice that the mAP cannot distinguish different attacks. For example, both the fabrication and vanishing attacks result in an $\text{mAP} \approx 0$, but they serve different attacking purposes (see Figure 5a).

Besides, the overall detection error includes attack error ϵ_{attack} and model error ϵ_{model} . The mAP measures the overall error by comparing the adversarial outputs with the ground truth, but we are only interested in the attack error.

$$\begin{aligned} \mathcal{O}(x') - \mathcal{O}_{\text{true}} &= [\mathcal{O}(x') - \mathcal{O}(x)] + [\mathcal{O}(x) - \mathcal{O}_{\text{true}}] \\ &= \epsilon_{\text{attack}} + \epsilon_{\text{model}} \end{aligned} \quad (9) \quad (10)$$

As a result, we devise three new evaluation metrics for the following experiments:

- 1) Mean Confidence Variation: The average increase or decrease of the confidence value of all the bounding boxes at each iteration step. This metric reflects the strength of the attack on the confidence value and be expressed as $\frac{1}{n-1} \sum_{i=2}^N (\hat{c}_i - \hat{c}_{i-1})$.
- 2) Number of Boxes: The total number of bounding boxes after the NMS. This metric shows how many objects are detected at each step of the attack $|\text{NMS}(\mathcal{O}_i(x'))|$.
- 3) Relative Box Variation: At each iteration, the position of false positive bounding boxes fluctuates. This metric measures the percentage of consistent bounding boxes at the current step and can be expressed as $\frac{|\text{NMS}(\mathcal{O}_i(x'))| + |\text{NMS}(\mathcal{O}_{i-1}(x'))| - |\text{NMS}(\mathcal{O}_i(x'), \mathcal{O}_{i-1}(x'))|}{|\text{NMS}(\mathcal{O}_i(x'))|}$.

The attackers' objective is to achieve a strong attack. We find that the adversarial loss determines the type of the attack (fabrication or vanishing), while it is the iteration process that determines the strength of the attack. Thus, we use our new evaluation metrics to study the iteration process to achieve stronger attacks against one-stage detection models (YOLO).

B. Initialization Method

We notice that the TOG attack [12] uses uniform initialization, while other attacks [10] [13] [14] [20] use zero initialization. Gradient-based attacks hinge on gradients to iterate from the original image to an adversarial input. Intuitively, uniform initialization may counteract the gradient at the first step. We conduct 5 runs of the PCB attack using uniform initialization, and compare the results with zero-initialization (see Fig. 6).

The third evaluation metric, relative box variation, converges to 1, indicating all false positive bounding boxes are stable. Different initialization methods result in similar convergence speeds. The first and second evaluation metrics, mean confidence variation and number of boxes, measure the strength of the attack. Only one in five runs of uniform initialization achieves a stronger attack than zero initialization. We confirm our hypothesis that uniform initialization counteracts the initial gradients.

C. Learning Rate Decay

To achieve a strong attack, we need to avoid gradient counteraction. The uniform initialization counteracts the initial gradients, and gradients at later iteration steps can cancel each other. Thus, the PCB attack introduces the learning rate decay k to solve this problem.

The original PGD attack does not include the learning rate decay ($k = 1.00$). As a result, the iteration process is stochastic (the black line in Figure 7), making it difficult to achieve a strong attack. This problem is not studied in prior research because they use the mAP as the evaluation metric. Even though the iteration process is stochastic, the value of mAP is low and stable. For example, at each step, we generate different false positive bounding boxes at various positions, but none of them matches the ground truth ($\text{mAP}=0$). As a result, even though the location of bounding boxes is stochastic, the mAP is as stable as 0.

Using our new evaluation metrics, we can see the complete iteration process (see Figure 7). As the learning rate decay k decreases from 0.99 to 0.90, it takes more steps for the two evaluation metrics, the mean confidence variation and the number of boxes, to converge. But they both converge at higher values, indicating a stronger attack.

As a result, the learning rate decay is necessary to achieve strong adversarial attacks.

D. Adversarial Loss Function

We further compare three adversarial loss functions of the fabrication attack. Our objective is not to find the best loss function but to highlight the advantages and disadvantages of different methods using our evaluation metrics.

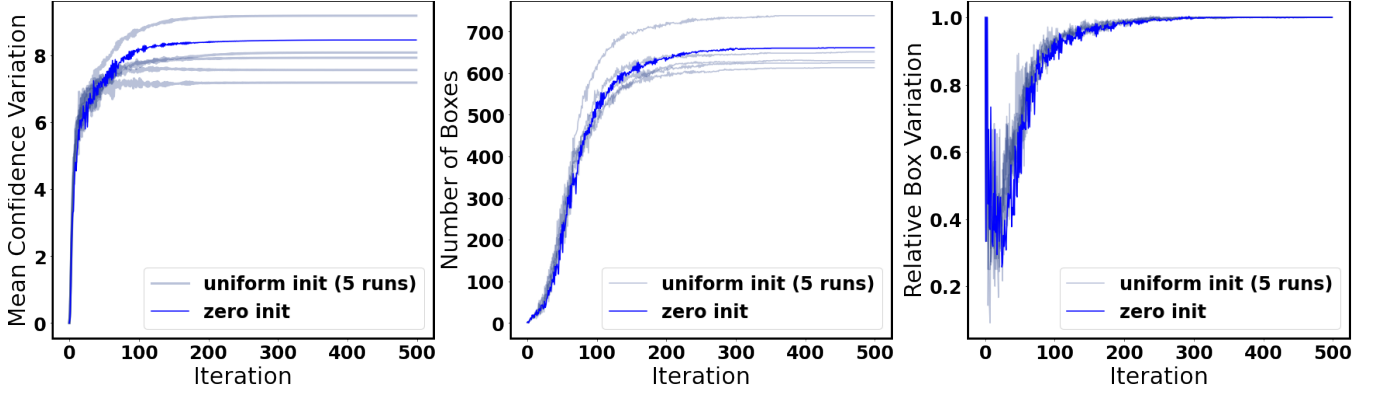


Fig. 6: The PCB fabrication attack using different initialization methods

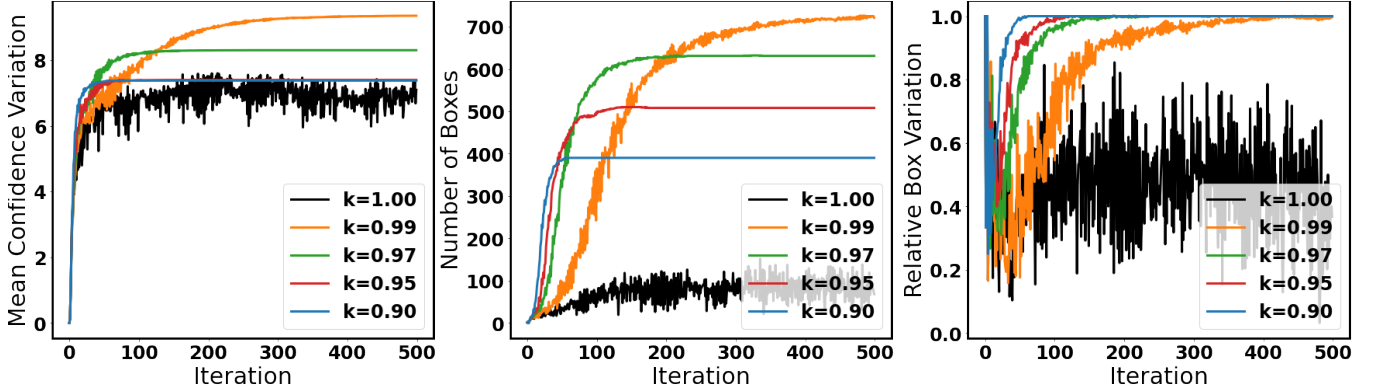


Fig. 7: The PCB fabrication attack with different learning rate decay

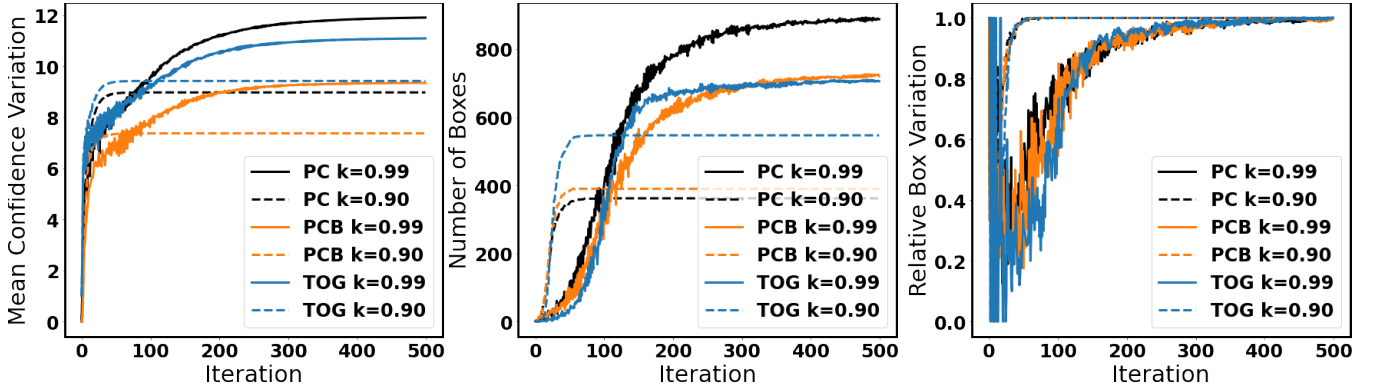


Fig. 8: Different adversarial loss functions of the fabrication attack

In Figure 8, the Relative Box Variation of all the three methods converges to 1, indicating locations of almost all the bounding boxes are stable at the end of the iteration. Though the PC attack generates the most bounding boxes and achieves the highest Mean Confidence Variation when $k = 0.99$, it takes more steps to reach the plateau. If the number of available sample images X_s is large, the PC attack requires more computational resources and time. On the other hand, the TOG and the PCB attack prevail over the PC attack when $k = 0.90$, and they converge faster.

As a result, we cannot conclude that a single method prevails over the others. Instead, our evaluation metrics are good references for decision-making.

V. CONCLUSIONS

In conclusion, it is possible to attack object detection models in embedded systems. We can generate a strong Universal Adversarial Perturbation and deploy the perturbation via the Man-in-the-Middle attack to fool the detection system.

In the future, we can integrate the perturbation into the camera and build an adversarial camera that fools deep-learning-enabled detection systems. Furthermore, this attack is not limited to object detection systems. We can generalize the Man-in-the-Middle attack to other sensors such as Lidar.

Is deep learning secure for robots? Perhaps not for safety-critical applications.

REFERENCES

- [1] I. Goodfellow, J. Shlens, and C. Szegedy, "Explaining and harnessing adversarial examples," in *International Conference on Learning Representations (ICLR)*, 2015.
- [2] J. Lu, H. Sibai, E. Fabry, and D. A. Forsyth, "No need to worry about adversarial examples in object detection in autonomous vehicles," in *Proceedings of the IEEE Conference on Computer Vision and Pattern Recognition (CVPR)*, 2017.
- [3] M. Lee and Z. Kolter, "On physical adversarial patches for object detection," *arXiv preprint arXiv:1906.11897*, 2019.
- [4] K. Xu, G. Zhang, S. Liu, Q. Fan, M. Sun, H. Chen, P.-Y. Chen, Y. Wang, and X. Lin, "Adversarial t-shirt! evading person detectors in a physical world," in *European Conference on Computer Vision (ECCV)*, 2020, pp. 665–681.
- [5] Z.-Q. Zhao, P. Zheng, S.-T. Xu, and X. Wu, "Object detection with deep learning: A review," *IEEE Transactions on Neural Networks and Learning Systems*, vol. 30, no. 11, pp. 3212–3232, 2019.
- [6] J. Redmon, S. Divvala, R. Girshick, and A. Farhadi, "You only look once: Unified, real-time object detection," in *Proceedings of the IEEE conference on computer vision and pattern recognition*, 2016, pp. 779–788.
- [7] W. Liu, D. Anguelov, D. Erhan, C. Szegedy, S. Reed, C.-Y. Fu, and A. C. Berg, "Ssd: Single shot multibox detector," in *European conference on computer vision*. Springer, 2016, pp. 21–37.
- [8] S. Ren, K. He, R. Girshick, and J. Sun, "Faster r-cnn: Towards real-time object detection with region proposal networks," *Advances in neural information processing systems*, vol. 28, 2015.
- [9] K. He, G. Gkioxari, P. Dollár, and R. Girshick, "Mask r-cnn," in *Proceedings of the IEEE international conference on computer vision*, 2017, pp. 2961–2969.
- [10] V. Fischer, M. C. Kumar, J. H. Metzen, and T. Brox, "Adversarial examples for semantic image segmentation," *arXiv preprint arXiv:1703.01101*, 2017.
- [11] R. Gurbaxani and S. Mishra, "Traits & transferability of adversarial examples against instance segmentation & object detection," *arXiv preprint arXiv:1808.01452*, 2018.
- [12] K.-H. Chow, L. Liu, M. Loper, J. Bae, M. E. Gursoy, S. Truex, W. Wei, and Y. Wu, "Adversarial objectness gradient attacks in real-time object detection systems," in *2020 Second IEEE International Conference on Trust, Privacy and Security in Intelligent Systems and Applications (TPS-ISA)*. IEEE, 2020, pp. 263–272.
- [13] D. Li, J. Zhang, and K. Huang, "Universal adversarial perturbations against object detection," *Pattern Recognition*, vol. 110, p. 107584, 2021.
- [14] O. Mohamad Nezami, A. Chaturvedi, M. Dras, and U. Garain, "Pick-object-attack: Type-specific adversarial attack for object detection," *Comput. Vis. Image Underst.*, vol. 211, no. C, oct 2021.
- [15] A. S. Hashemi, A. Bär, S. Mozaffari, and T. Fingscheidt, "Transferable universal adversarial perturbations using generative models," *arXiv preprint arXiv:2010.14919*, 2020.
- [16] X. Wei, S. Liang, N. Chen, and X. Cao, "Transferable adversarial attacks for image and video object detection," in *Proceedings of the Twenty-Eighth International Joint Conference on Artificial Intelligence, IJCAI-19*. International Joint Conferences on Artificial Intelligence Organization, 7 2019, pp. 954–960.
- [17] N. Carlini and D. Wagner, "Towards evaluating the robustness of neural networks," in *2017 IEEE Symposium on Security and Privacy (SP)*. IEEE, 2017, pp. 39–57.
- [18] Q. Liao, X. Wang, B. Kong, S. Lyu, B. Zhu, Y. Yin, Q. Song, and X. Wu, "Transferable adversarial examples for anchor free object detection," in *2021 IEEE International Conference on Multimedia and Expo (ICME)*. IEEE, 2021, pp. 1–6.
- [19] N. Bodla, B. Singh, R. Chellappa, and L. S. Davis, "Soft-nms improving object detection with one line of code," in *Proceedings of the IEEE international conference on computer vision*, 2017, pp. 5561–5569.
- [20] A. Madry, A. Makelov, L. Schmidt, D. Tsipras, and A. Vladu, "Towards deep learning models resistant to adversarial attacks," *arXiv preprint arXiv:1706.06083*, 2017.
- [21] J. Cartucho, R. Ventura, and M. Veloso, "Robust object recognition through symbiotic deep learning in mobile robots," in *2018 IEEE/RSJ International Conference on Intelligent Robots and Systems (IROS)*, 2018, pp. 2336–2341.